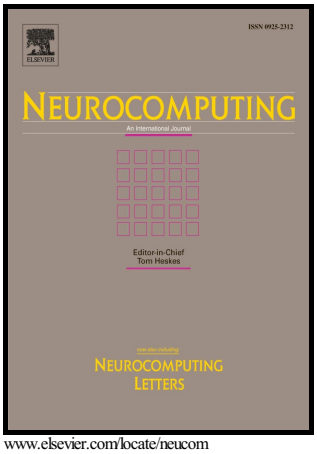

www.elsevier.com/locate/neucom

Integration of touch attention mechanisms to improve the robotic haptic exploration of surfaces

Ricardo Martins, João Filipe Ferreira, Miguel Castelo-Branco, Jorge Dias

PII: S0925-2312(16)31218-8
DOI: http://dx.doi.org/10.1016/j.neucom.2016.10.027
Reference: NEUCOM17639

To appear in: *Neurocomputing*

Received date: 21 February 2016
Revised date: 11 July 2016
Accepted date: 17 October 2016

Cite this article as: Ricardo Martins, João Filipe Ferreira, Miguel Castelo-Branc and Jorge Dias, Integration of touch attention mechanisms to improve the roboti haptic exploration of surfaces, *Neurocomputing* http://dx.doi.org/10.1016/j.neucom.2016.10.027

Integration of touch attention mechanisms to improve the robotic haptic exploration of surfaces

Ricardo Martins[a,b], João Filipe Ferreira[a], Miguel Castelo-Branco[b], Jorge Dias[a,c]

[a] *ISR-UC, Institute of Systems and Robotics*
Department of Electrical and Computer Engineering - University of Coimbra Polo II, 3030-290 Coimbra-Portugal
{rmartins, jfilipe, jorge}@isr.uc.pt
[b] *IBILI-UC, Institute for Biomedical Imaging and Life Sciences*
Faculty of Medicine, University of Coimbra, Coimbra, Portugal
mcbranco@fmed.uc.pt
[c] *Robotics Institute, Khalifa University, Abu Dhabi, UAE*

Abstract

This text presents the integration of touch attention mechanisms to improve the efficiency of the action-perception loop, typically involved in active haptic exploration tasks of surfaces by robotic hands. The progressive inference of regions of the workspace that should be probed by the robotic system uses information related with haptic saliency extracted from the perceived haptic stimulus map (*exploitation*) and a "curiosity"-inducing prioritisation based on the reconstruction's inherent uncertainty and inhibition-of-return mechanisms (*exploration*), modulated by top-down influences stemming from current task objectives, updated at each exploration iteration. This work also extends the scope of the top-down modulation of information presented in a previous work, by integrating in the decision process the influence of shape cues of the current exploration path. The Bayesian framework proposed in this work was tested in a simulation environment. A scenario made of three different materials was explored autonomously by a robotic system. The experimental results show that the system was able to perform three different haptic discontinuity following tasks with a good structural accuracy, demonstrating the selectivity and generalization capability of the attention mechanisms. These experiments confirmed the fundamental contribution of the haptic saliency cues to the success and accuracy of the execution of the tasks.

Keywords: touch attention; artificial perception; Bayesian modelling; path planning; haptic exploration; probabilistic grid maps;

1. Introduction

In an attempt to capitalise on the same advantages that having hands benefit human beings, researchers have recently put a lot of effort into the development of dexterous robotic hands, due to the mechanical (high number of degrees-of-freedom) and sensory (tactile, force, torque, heat) capabilities that they provide. These devices allow robotic platforms to perform precise manipulation of objects (reaching, grasping, transportation, in-hand reorientation) [1], as well as haptic exploration of surfaces using different patterns of movements (lateral motion, press-and-release, static contact), thereby promoting the extraction and integration of different haptic properties (contours, texture, compliance, temperature) of the materials these surfaces are composed of [2].

The contributions presented in this work are related with the robotic haptic exploration of surfaces, following three essential assumptions: (1) no other type of sensors are used besides haptics (i.e. exploration is "blind"); (2) exploration paths are not predefined; (3) the surface geometry is unknown to the robot. The objectives of the exploration tasks concern haptic discontinuity/contour following. Haptic discontinuities are defined by the transition/border regions between surfaces with different haptic properties. During haptic exploration, the interaction of

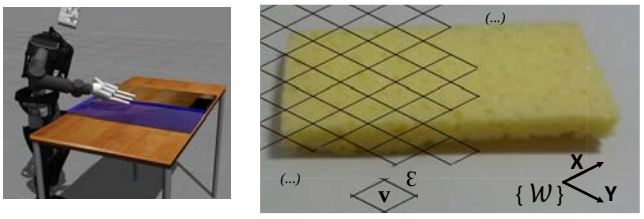

(a) (b)

Figure 1: a) Results from a previous work [3], demonstrating a haptic discontinuity following task: straight line geometry. In this work, the haptic exploration tasks are more challenging: three materials and discontinuities with other geometries than straight lines. b) Illustration of a 2D isometric grid partitioning a real world workspace area. Each cell $\mathbf{v}$ has a dimension ε and is described by position (x, y) expressed in $\{\mathcal{W}\}$.

the robotic platform with the probed surface provides multiple simultaneous streams of data over its geometry and the properties of its composing materials relayed by an ensemble of haptic sensors. This data is potentially uncertain due to sensor noise and the unknown nature of the surface.

To tackle these challenges, we propose a Bayesian framework to implement autonomous haptic exploration of surfaces that implements an action-perception loop architecture. The Bayesian formalism provides a principled way of implementing the integration of the multimodal sensory data supplied by the haptics ensemble while properly dealing with their inherent uncertainty. The proposed action-perception loop architecture integrates touch attention mechanisms (i.e. stimulus-driven processes modulated by task-relevant top-down influences) to optimise the exploration strategy. This in turn promotes adaptive behaviour due to the exploration and exploitation traits of such mechanisms.

The haptic exploration of surfaces plays a fundamental role in reduced visibility scenarios (i.e.: underwater robotic manipulation, smoky and foggy disaster environments, partial or complete occlusion of elements in the scenario). Although this work only addresses the implementation of haptic exploration strategies, the proposed Bayesian framework allows the integration of additional sensory sources such as vision (depth, color) and laser to infer the robotic exploration path. The approach proposed in this work can be used to complement methods already available to explore surfaces using exclusively non-haptic sensory inputs [4] [5] [6].

The structure of the manuscript and an overview of the Bayesian models proposed in this work are presented in section 1.1.

1.1. Problem formulation and approach overview

In the application scenarios used in this work, the exploration task is performed on top of a table – a workspace defined by a planar surface – and using a generic robotic system with manipulation capability. The internal structure and configuration of the workspace is unknown *a priori* to the robotic system. The solution to the haptic exploration task is described in two-dimensional Cartesian space, progressively unfolding a sequence of regions of the workspace to be probed by the robotic platform during task execution.

As in previous reported work, the 2D-Cartesian space is partitioned using a planar isometric 2D grid (square cells), as represented in Fig. 1 b). Each cell v_k has a side of length ε and is described by a 2D Cartesian location (x,y) expressed in the inertial world referential $\{\mathscr{W}\}$. These tesselations of space have been used extensively in robotics as inference grids in many applications [9].

The methods presented follow the principles and architecture of the human somatosensory processing pipeline and human cognition. A conceptual overview of our solution is presented in Fig. 2; the corresponding detailed diagram is given in Fig. 3, including a representation of data flow. Haptic sensory inputs are acquired during the local interaction of the robotic exploratory elements with the environment at region $\mathbf{v}_k$. Haptic

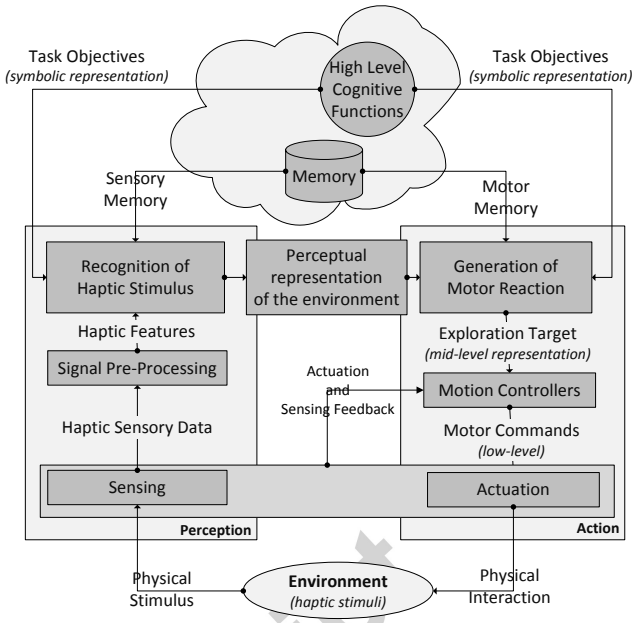

Figure 2: Conceptual representation of the action-perception loop [7] involved in the haptic exploration of surfaces [8]. In this work, the objectives of the task and corresponding solution is represented in two levels: symbolic and mid-level.

features such as texture, compliance, temperature are extracted from the haptic sensory inputs. These features are integrated and used to discriminate the different classes of materials in the workspace. These processes are modelled by the Bayesian model π_{per} presented in section 3.

Next in the sensory processing pipeline, the robotic system uses the updated perceptual representation of the workspace to infer the next region that should be explored. The mechanisms involved in this process are implemented by the Bayesian model π_{tar} and described in section 5. Touch attention is modelled by integrating the following:

- **Stimulus-driven processes** – concurrent mechanisms that promote both *exploitation* behaviour concerning perceptual representations of stimuli in the form of haptic saliency and shape cues (determined by the Bayesian model π_{obj}, section 4), and *exploration* behaviours fuelled by spatial distribution of perceptual uncertainty and also inhibition-of-return mechanisms.
- **Goal-directed modulation** – mechanisms that influence the weights of stimulus-driven processes through top-down influences informed by current task objectives.

The experimental setup used in this work is described in section 6. The impact of the integration of the touch attention mechanisms in the action-perception loop and generalization capability of the exploration strategies inferred from the proposed Bayesian models are tested in simulation environment, section 6. The main conclusions of this work and formulation of the main guidelines for future developments of this approach are presented in section 7.

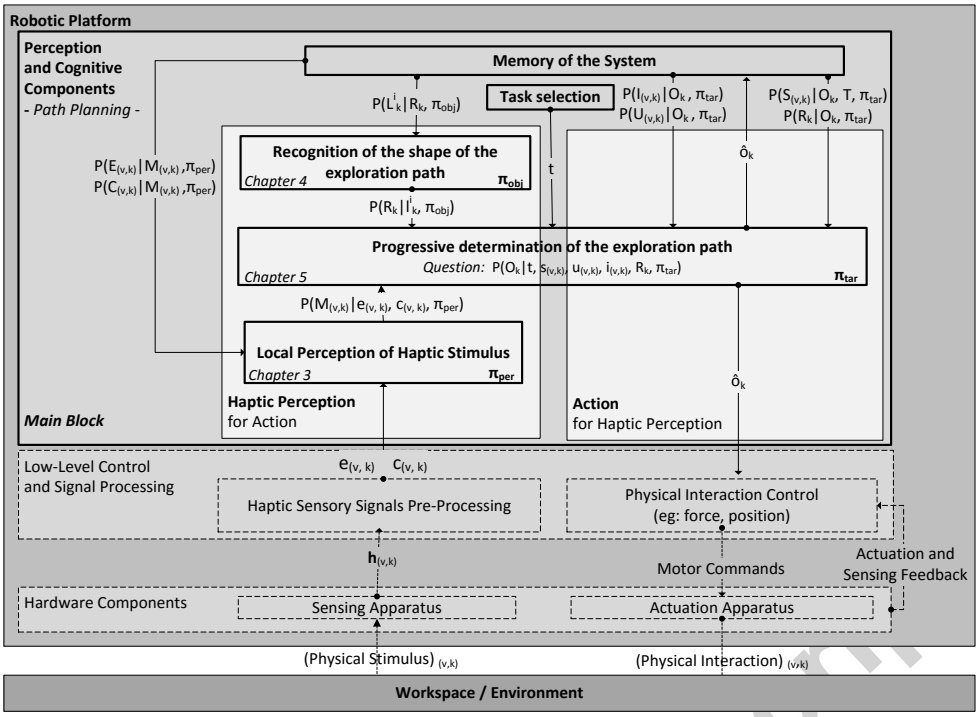

Figure 3: Detailed diagram of the architecture of the proposed system. The main contributions of this work are identified in the diagram as *main block* (local perception of haptic stimulus, recognition of the shapes of discontinuities, progressive determination of the exploration path). The variables of the system are summarised in table 1.

1.2. Path planning of the global haptic exploration strategy

The framework conceptually represented in Fig. 2 and detailed in Fig. 3 implements a haptic exploration path planning method, which infers a series of global via-points in the workspace that should be probed by the robotic system.

This work does not address the low-level control loop involved in physical interaction of the fingers with the surface and the ability to move the fingers along the surface by keeping contact. In other words, the low-level modelling and control of local contact interaction (eg: force, impedance, position control) and processing of haptic sensory data are not discussed by this work. These processes are implemented in Fig. 3 by the module *Low-Level Control and Signal Processing* and inner loop labelled *Actuation and Sensing Feedback*.

Our solution assumes that algorithms (dependent of specific robotic device and sensing apparatus) implemented by other works (eg: [10]) extract different haptic features and control the local movements during the haptic exploration of a region $\mathbf{v}_k$. The integration between these lower level control models (dashed boxes) and the global exploration path planning method (bold boxes) proposed by this work is detailed in Fig. 3.

Table 1: Summary of the relevant variables of this work.

Variable	Description	Domain
v	Cell of the workspace grid.	$\mathbb{R}^2$
k	Time / exploration iteration.	$\mathbb{N}_0$
R_k	Category of the structure of the discontinuity.	$\{"Shape_1","Shape_2"\}$
$template_i$	Set of points defining the template of each category of structure.	$\mathbb{R}^2$
L^i_k	Matching error between the exploration path and $template_i$.	[0,1]
$M_{(v,k)}$	Material category of v	$\{Material_1,\ldots,Material_{10}\}$
$E_{(v,k)}$	Texture characterization of v.	$\mathbb{R}$
$C_{(v,k)}$	Compliance characterization of v.	$\mathbb{R}$
$\mathbf{h}_{(v,k)}$	Raw haptic sensing data acquired on v.	$\mathbb{R}^n$ *
O_k	Next workspace region to be explored.	v
$I_{(v,k)}$	Inhibition level for cell v.	$[0,1]$
$U_{(v,k)}$	Uncertainty level for cell v.	$[0,1]$
$S_{(v,k)}$	Saliency of the perceived haptic stimulus in region v.	$[0,1]$
T	Objective of the haptic exploration task.	$\{T_1,T_2,T_3\}$

2. Related works

The robotic exploration of surfaces using haptic inputs has been a research topic pursued for a long time, with seminal works by [23], [24], [25] and [26].

Table 2: Comparison between the contributions of this work and the related works

Study	**Apparatus** [a]	**Local Haptic Perception**		**Global Exploration of the workspace**			
		Approach [b]	Features [c]	Approach [d]	Task [e]	Strategy [f]	Workspace [g]
This Work	HS	P	T, CO	P	M:E, F:E	AE	GD:2D
[11]	HS	D	C	-	-	-	-
[12]	HS	D	T	-	-	-	-
[10]	HS	P	CO, T, TC	-	-	-	-
[13]	HS	P	T	-	-	-	-
[14]	HS	D	T	-	-	-	-
[15]	HS	P	C	-	-	-	-
[16]	HS	P	S	-	-	-	-
[17]	HS	D	C, TC	-	-	-	-
[18]	HS	D	CO	D	M:C	PD	CS:2D
[19]	HS	D	RO	P	F:T	PD	-
[20]	HS	P	C	D	F:C	AE	-
[21]	HS, VS	P	TO	P	M:E	AE	GD:2D
[22]	HS	P	RO	D	M:E, F:E	AE	GD:2D
[20]	HS	D	CI, CR	D	F	AE	CS:3D

[a] HS- haptic sensing; VS- visual sensing.
[b],[d] P- probabilistic; D- deterministic.
[c] T- texture; CO- compliance; C- curvature; TC- thermal conductivity; S- stickiness; RO- raw sensory output; CI- contact intensity; CR- contact orientation.
[e] M:E- mapping edge; M:C - mapping compliance; F- following; F:E- following edge; F:T- following texture; F:C: following curvature;
[f] AC- active exploration; PD- pre-defined exploration path.
[g] GD:2D - bi-dimensional grid; CS:2D- bi-dimensional Cartesian space points; CS:3D- tri-dimensional Cartesian space points;

A group of approaches described in the literature implements haptic exploration by attempting to achieve a single categorisation of surfaces or objects. The exploration is performed locally in a specific region, considering that it is representative of the whole surface by assuming that the latter is either homogeneous or uniform in terms of the haptic features under analysis. The discrimination between the different classes of surfaces is performed by extracting distinct but complementary types of haptic features such as surface curvature [11], texture [12] [10] [13] [14], compliance [15] [10], stickiness [16] and thermal conductivity [10] [17] from the haptic sensory signals. The formalisation of the descriptors of the haptic features depends on the type of robotic platform and type of sensing apparatus involved in the exploration task, specifically the modelling of the contact interaction and the characteristics of the sensory signals produced during that interaction. However, each type of haptic feature is extracted using the same exploration movement patterns across the different works.

The work presented in this manuscript contributes to this group of approaches by introducing a Bayesian model that allows the discrimination different categories of materials through the integration of compliance and texture features. The formulation of haptic features abstracts the contact interaction models between the exploratory element and the surface.

A second group of approaches, while integrating sensing, perception and local exploration mechanisms similarly to the previous group, expands the exploration strategy to large and heterogenous surfaces in the haptic feature domain under analysis. The global perceptual map of the surface can be constructed following different strategies. In many proposed solutions, the global exploration path is fixed and defined *a-priori*. For example, in [18], haptic exploration is performed using pre-defined exploration paths to build a stiffness map of biological tissues. As long as the perception of the haptic stimulus of the surface occurs, it does not influence the exploration movement. In [19], Braille symbols are explored and recognised by a robotic system. The exploration speed is adjusted depending on the recognition uncertainty, nevertheless the exploration path is also predefined.

Although exploration strategies defined *a-priori* can be successful when substantial information about the structure of the environment is available, in most of the scenarios identified considering the motivation behind this work, the structure of the environment is initially unknown (partially or completely). Thus, the exploration strategy should introduce an active behaviour to progressively integrate and analyse the local perceptual representation of the environment (*perception for action*) and estimate what should be the next global region to explore and perceive (*action for perception*), as proposed in [27]. Active exploration of a scene represented by a occupancy grid was proposed by [21]. An initial estimation of the scene structure is made using stereovision data and projected in a 2D occupancy grid. The exploration strategy is dependent of that initial representation and haptic inputs (lateral contact/non-contact) are used to confirm and update the occupancy grid of the map.

In other works, the active exploration task is started without any knowledge about scene structure. For example, [22] proposes a method to perform active contour following of objects by performing tap movements using a robotic fingertip equipped with a tactile array. The reaction of the system is formulated based on the contact profile between the haptic stimulus and the tactile sensing array and specific deterministic rules defined beforehand by the human operator. [20] presents a generic formulation of a control framework for different types of tasks that require tactile servoing (eg: tracking a touched object, tactile object active exploration). Different behaviours are obtained by adjusting a few matrix parameters and selecting the corresponding haptic primitives extracted from a tactile array.

This work adds to the contributions of this class of approaches by proposing a formulation of Bayesian models implementing touch attention mechanisms involved in the active haptic exploration of unknown surfaces by generic robotic hands and sensory apparatus. Once this work assumes that the workspace is unknown *a-priori* to the system (blind exploration), the ex-

ploration path is adapted actively by the touch attention mechanisms, as long as the exploration progresses. The definition of the architecture of the Bayesian models follows the principles on how humans manage uncertainty to make motor decisions from percepts [7], and extends the architecture proposed in a previous work [3]. The work presented in this manuscript expands the top-down modulation of information, by integrating an additional Bayesian model in the decision process, representing the influence of the shape of the current exploration path (detailed in section 4). In [3] the experimental results were focused on testing extensively the capability of the system to discriminate different type of materials. In the current work, a completely new set of experiments is designed to test the selectivity (different types of discontinuities) and robustness (different path shapes) of the touch attention mechanisms during three haptic discontinuity following tasks. The new experimental design was also used to evaluate the contributions of the different types of cues modelled by the Bayesian models to the performance of the robotic system.

3. Local perception of haptic stimulus map

3.1. Random variables of the model

The type of material describing workspace region v is represented by the discrete random variable $M_{(v,k)}$, defined as follows:

$$M_{(v,k)} \in \{Material_1, \ldots, Material_{10}\}. \quad (1)$$

During local exploration of region v of the workspace at time iteration step k, the robotic system acquires haptic sensory data represented by variable $\mathbf{h}_{(v,k)}$. The categories of materials are discriminated according to different properties of texture and compliance, hence haptic sensory inputs $\mathbf{h}_{(v,k)}$ are used to determine the category of material describing the cell v of the workspace. Haptic sensing measurements $\mathbf{h}_{(v,k)}$ are transformed using function g into a compliance characterisation of the explored surface, and using function f into a texture characterization of the surface. This work considers the same operator functions f and g of the work [10]. The texture and compliance characteristics of the region v of the workspace are described by the continuous random variables, $E_{(v,k)} \equiv$"Texture characterization of v", and $C_{(v,k)} \equiv$"Compliance characterization of v", respectively, according to the following expressions:

$$\begin{aligned} E_{(v,k)} &= f(\mathbf{h}_{(v,k)}), \quad E_{(v,k)} \in \mathbb{R}, \\ C_{(v,k)} &= g(\mathbf{h}_{(v,k)}), \quad C_{(v,k)} \in \mathbb{R}. \end{aligned} \quad (2)$$

3.2. Inference of the haptic stimulus category

The Bayesian model π_{per} allowing the estimation of surface material given haptic sensory inputs (Fig. 4) was extensively tested in previous work [3], in which it was used to discriminate between different classes of materials (the same set of 10 different classes used in the work presented in [10], more specifically acrylic, brick, copper, damp sponge, feather, rough foam,

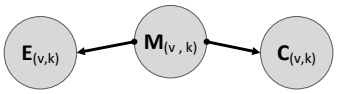

(a)

Bayesian Program

Description

Specification

Relevant variables:

$E_{(v,k)}, C_{(v,k)}, M_{(v,k)}$

Decomposition:

$$P(E_{(v,k)}, C_{(v,k)}, M_{(v,k)}|\pi_{per}) = \left(\begin{array}{c} P(E_{(v,k)}|M_{(v,k)}, \pi_{per}).P(C_{(v,k)}|M_{(v,k)}, \pi_{per}). \\ .P(M_{(v,k)}|\pi_{per}) \end{array}\right)$$

Parametric forms:

$P(E_{(v,k)}|M_{(v,k)}, \pi_{per}) \equiv \mathcal{N}(\mu_E(M), \sigma_E(M))$

$P(C_{(v,k)}|M_{(v,k)}, \pi_{per}) \equiv \mathcal{N}(\mu_C(M), \sigma_C(M))$

For $k = 0$:

Map initialization.

$P(M_{(v,0)}|\pi_{per}) \equiv$ *Uniform*

For $k > 0$:

Map update using previous state information.

$P(M_{(v,k)}|\pi_{per}) =$

$P(M_{(v,k-1)}|e_{(v,k-1)}, c_{(v,k-1)}, \pi_{per})$

Identification:

$\mu_E(M), \sigma_E(M), \mu_C(M), \sigma_C(M)$

- *Constants defined during the learning stage.*

Question:

$P(M_{(v,k}|e_{(v,k)}, c_{(v,k)}, \pi_{per})$

(b)

Figure 4: Bayesian model π_{per}:*"Local perception of haptic stimulus"*. a) Graphical representation. b) Description of the Bayesian program.

plush toy, silicone, soft foam, wood) with an average recognition rate higher than 90%, even when sensory samples were corrupted with Gaussian white noise. These categories of materials are characterised by different properties of texture, compliance and thermal conductivity that were extracted using *BioTac* biomimetic tactile sensor raw data (contact intensity, vibration, heat flow). In our work, we only consider texture and compliance properties of the materials.

The conditional independence relations between random variables $E_{(v,k)}, C_{(v,k)}, M_{(v,k)}$ are expressed in Fig. 4 a). Based on these assumptions, the joint probability distribution function $P(E_{(v,k)}, C_{(v,k)}, M_{(v,k)}|\pi_{per})$ is decomposed as described in Fig. 4 b), with respective parametric forms.

At each time step, the probability distribution function $P(M_{(v,k)}|e_{(v,k)}, c_{(v,k)}, \pi_{per})$ describing the probability of the surface at v corresponding to each material category is inferred using the observed data $e_{(v,k)}, c_{(v,k)}$ extracted from the samples acquired by the sensory apparatus of the robotic system:

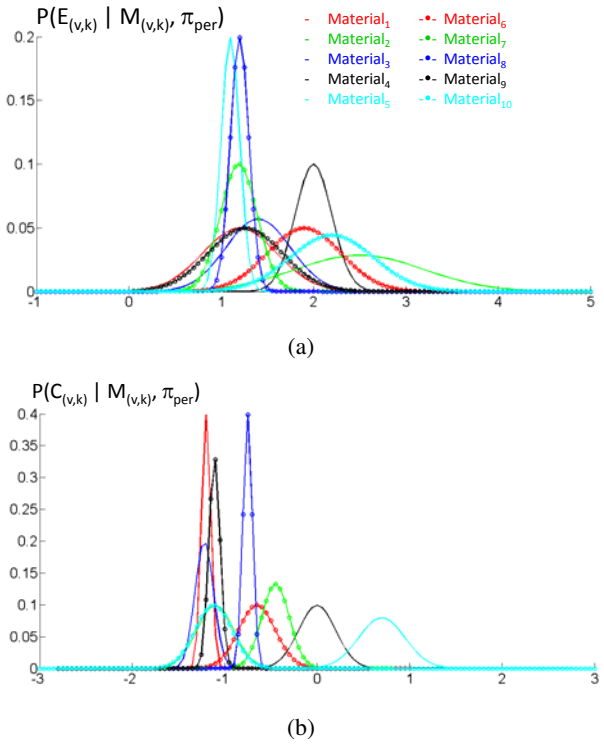

Figure 5: Representation of $P(E_{(vi,k)}|M_{(vi,k)},\pi_{per})$ (a)) and $P(C_{(vi,k)}|M_{(vi,k)},\pi_{per})$ (b)) learned for 10 reference materials. Data extracted from [10].

$$P(M_{(v,k)}|e_{(v,k)},c_{(v,k)},\pi_{per}) = \frac{\begin{pmatrix} P(e_{(v,k)}|M_{(v,k)},\pi_{per}). \\ P(c_{(v,k)}|M_{(v,k)},\pi_{per}).P(M_{(v,k)},\pi_{per}) \end{pmatrix}}{\sum_{M_{(v,k)}} \begin{pmatrix} P(e_{(v,k)}|M_{(v,k)},\pi_{per}). \\ P(c_{(v,k)}|M_{(v,k)},\pi_{per}).P(M_{(v,k)},\pi_{per}) \end{pmatrix}} \quad (3)$$

3.3. Determination of $P(E_{(v,k)}|M_{(v,k)},\pi_{per})$ and $P(C_{(v,k)}|M_{(v,k)},\pi_{per})$

The parameters $\mu_E(M)$, $\sigma_E(M)$, $\mu_C(M)$, $\sigma_C(M)$ of the Gaussian functions modelling the Normal probability distributions $P(E_{(v,k)}|M_{(v,k)},\pi_{per})$ and $P(C_{(v,k)}|M_{(v,k)},\pi_{per})$ are estimated during experimental learning sessions using a maximum-likelihood procedure. As described in [10], during the learning period, standard local exploration procedures are performed for each of the $n = 10$ reference materials.

After the pre-determined number of standard local explorations, the free parameters $\mu_E(M)$, $\sigma_E(M)$, $\mu_C(M)$, $\sigma_C(M)$ of the Normal ($\mathcal{N}$) distributions are determined by calculating the averages μ and standard deviations σ of E and C for each reference material. The resulting $P(E_{(v,k)}|M_{(v,k)},\pi_{per})$ and $P(C_{(v,k)}|M_{(v,k)},\pi_{per})$ are represented in figures 5 a) and 5 b), extracting the data available from the manuscript of the work [10].

4. Recognition of the shape of the global exploration path

4.1. Random variables of the model

As the haptic exploration of the workspace progresses, the exploration path is described by the set of regions of the two-dimensional workspace grid probed by the robotic system. The shape of the exploration path provides cues that can be recognised by the haptic exploration framework.

The category of the shape of the exploration path is represented by discrete random variable R_k, defined as follows:

$$R_k \in \{Shape_1,\ldots,Shape_\Theta\}. \quad (4)$$

Each class of shape described by discrete random variable R_k is associated with a template, represented by a set of points $template_i$,

$$\forall_{i\in\{1,\ldots,\Theta\}} \quad \langle \text{"}Shape_i\text{"}, template_i\rangle. \quad (5)$$

This work assumes that the robotic system is able to recognize $\Theta = 2$ categories of shapes: a rectangle and a triangle, respectively.

The sequence of regions of the workspace explored by the robotic system until time step $(k-1)$ is described by the set of workspace locations $(\hat{o}_0,\hat{o}_1,\ldots,\hat{o}_{k-1})$ (section 5). The categorisation process consists of establishing a match between the points $(\hat{o}_0,\hat{o}_1,\ldots,\hat{o}_{k-1})$ explored by the robotic system until time step $(k-1)$ and each of the templates $template_i$, representative of each category of structure of discontinuity. The normalised matching error between each template and the current exploration path is described by the continuous random variable L^i, defined as follows:

$$[L^i,\Upsilon_i] = f_{ICP}((\hat{o}_0,\hat{o}_1,\ldots,\hat{o}_{k-1}),template_i), \quad L^i \in [0,1] \quad (6)$$

The matching between the two sets of points $(\hat{o}_0,\hat{o}_1,\ldots,\hat{o}_{k-1})$ and $template_i$ is determined using the *Iterative Closest Point* (ICP) method [28], as described in equation 6.

Besides matching error L^i, the ICP function f_{ICP} returns the estimation of the geometrical transformation Υ_i between the two sets of points. This transformation can be used to determine a new set of points $template_i^{'}$ which results from the registration of the $template_i$ points in the structure described by the set of points $(\hat{o}_0,\hat{o}_1,\ldots,\hat{o}_{k-1})$.

This relation can be described by the geometrical transformation represented in the following equation,

$$template_i^{'} = \Upsilon_i.template_i, \quad (7)$$

as used in section 5.

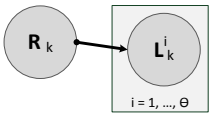

(a)

Bayesian Program
- Description
  - Specification
    - Relevant variables:
    - $R_k, L_k^1, \ldots, L_k^\Delta$
    - Decomposition:
    - $P(R_k, L_k^1, \ldots, L_k^\Delta | \pi_{obj}) =$
    - $P(L_k^1 | R_k, \pi_{obj}) \ldots . P(L_k^\Delta | R_k, \pi_{obj}) . P(R_k | \pi_{obj})$
    - Parametric forms:
    - $P(L_k^i | R_k, \pi_{obj}) \equiv \mathscr{B}(\alpha_{L^i}, \beta_{L^i})$
    - $P(R_k | \pi_{obj}) \equiv Uniform$
  - Identification:
  - $\alpha_{L^i}, \beta_{L^i}$
  - $-$*Constants defined empirically.*
- Question:
- $P(R_k | l_k^1, \ldots, l_k^\Delta, \pi_{obj})$

(b)

Figure 6: Bayesian model π_{obj}:*"Recognition of the shapes of discontinuities."*. a) Graphical representation. b) Description of the Bayesian program.

4.2. Inference of category of shape

The graphical representation of Bayesian model π_{obj} presented in Fig. 6 a) expresses the conditional independence relations between random variables $L_k^1, \ldots, L_k^\Theta, R_k$. According to these relations, the joint probability distribution function $P(L_k^1, \ldots, L_k^\Theta, R_k | \pi_{obj})$ can be factored as presented in Fig. 6 b).The probability distribution function followed by each of those factors is also presented in Fig. 6 b).

At each time step, the probability distribution function $P(R_k | l_k^1, \ldots, l_k^\Theta, \pi_{obj})$ is inferred using the Bayesian program of Fig. 6 through the following equation:

$$P(R_k | l_k^1, \ldots, l_k^\Theta, \pi_{obj}) = \frac{P(l_k^1 | R_k, \pi_{obj}) \ldots . P(l_k^\Theta | R_k, \pi_{obj}) . P(R_k | \pi_{obj})}{\sum_{R_k} P(l_k^1 | R_k, \pi_{obj}) \ldots P(l_k^\Theta | R_k, \pi_{obj}) P(R_k | \pi_{obj})} \quad (8)$$

4.3. Determination of $P(l_k^i | R_k, \pi_{obj})$

The probability distribution functions $P(l_k^i | R_k, \pi_{obj})$ are described by beta probability distribution functions $\mathscr{B}_L$ with the constant parameters $\alpha_L = 1.0$ and $\beta_L = 4.5$. All Θ probability distribution functions are assumed identical.

The typical profile of the probability distribution function $P(l_k^i | R_k, \pi_{obj})$ is represented in Fig. 8 b). The profile proposed for $P(l_k^i | R_k, \pi_{obj})$ attributes higher probabilities to lower levels of normalized matching errors l_k^i and lower probabilities to higher values of l_k^i. This promotes the selection of categories of the structure R_k that have a template similar to the current exploration path $(\hat{o}_0, \hat{o}_1, \ldots, \hat{o}_{k-1})$.

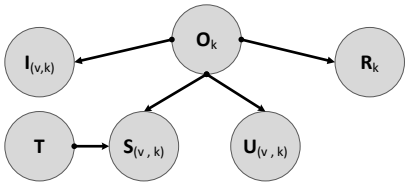

(a)

Bayesian Program
- Description
  - Specification
    - Relevant variables:
    - $O_k, T, S_{(v,k)}, U_{(v,k)}, I_{(v,k)}$
    - Decomposition:
    - $P(O_k, T, S_{(v,k)}, U_{(v,k)}, I_{(v,k)} | \pi_{tar}) =$
    - $\left(\begin{array}{l} P(O_k | \pi_{tar}) . P(T | \pi_{tar}) . P(I_{(v,k)} | O_k, \pi_{tar}) . \\ . P(U_{(v,k)} | O_k, \pi_{tar}) . P(S_{(v,k)} | O_k, T, \pi_{tar}) \end{array} \right)$
    - Parametric forms:
    - $P(O_k | \pi_{tar}) \equiv Uniform$
    - $P(T | \pi_{tar}) \equiv Uniform$
    - $P(I_{(v,k)} | O_k, \pi_{tar}) \equiv \mathscr{B}(\alpha_I, \beta_I)$
    - $P(U_{(v,k)} | O_k, \pi_{tar}) \equiv \mathscr{B}(\alpha_U, \beta_U)$
    - $P(S_{(v,k)} | O_k, T, \pi_{tar}) \equiv \mathscr{B}(\alpha_S, \beta_S)$
  - Identification:
  - $\alpha_I, \beta_I, \alpha_U, \beta_U, \alpha_S, \beta_S$
  - $-$*Constants defined empirically.*
- Question:
- $P(O_k | t, s_{(v,k)}, u_{(v,k)}, i_{(v,k)}, \pi_{tar})$
- Decision criteria: *MAP - Maximum a posteriori.*
- $\hat{o}_k = \arg\max_{o_k} P(O_k | t, s_{(v,k)}, u_{(v,k)}, i_{(v,k)}, \pi_{tar})$

(b)

Figure 7: Bayesianl model π_{tar}:*"Selection of the next exploration target"*. a) Graphical representation. b) Description of the Bayesian program.

5. Integration of touch attention mechanisms in the inference of the global exploration path

5.1. Random variables of the model

After the local exploration of the region v of the workspace is concluded, the perceptual representation of the workspace is updated with the sensory measurements acquired at v (update mechanisms presented in section 3), and the robotic system has to decide which region v of the workspace grid should be explored next (path planning of global exploration strategy).

The next exploration target is represented by the discrete random variable O_k, defined as

$$O_k \in \{v^1, v^2, v^3, \ldots, v^\theta\}, \quad (9)$$

in which θ is the total number of cells in the grid representation of the workspace, and v^i is a compact representation of the cell identifier.

Robotic platforms have been endowed with attentional mechanisms implemented in different sensory domains in order to

deal with sensory overload, prioritisation and dynamic environments [29].

The sequence of workspace regions $(\hat{o}_0, \hat{o}_1, \ldots, \hat{o}_{k-1})$ previously explored by robotic system, can provide cues about the shape of the discontinuity that is being followed and indirectly influence the estimation of $\hat{o}_k$. The cues are provided by matching the current structure of the exploration path, with representations of typical shapes stored in the memory of the robotic system. As presented in section 5.3, unexplored regions of the workspace that are coincident with the structure of the shape templates will be more likely to be explored.

The selection of O_k is also conditioned by inhibition-of-return mechanisms. The inhibition level imposed this mechanism to the overall attention process is implemented by the continuous random variable $I_{(v,k)}$ ="Inhibition level for cell v" as follows:

$$I_{(v,k)} = 1 - \Theta d^{\alpha-1}(1-d)^{1-\beta}, \quad I_{(v,k)} \in [0,1] \qquad (10)$$

Due to the characteristics of the haptic exploration procedures presented in section 1, at time step $k+1$ the inhibition-of-return process promotes the exploration of regions of the workspace different from the current position of the end-effector of the robotic system ($\hat{o}_{k-1}$), therefore avoiding deadlocks. However, simultaneously, the inhibition-of-return process inhibits the exploration of regions too distant from $\hat{o}_{k-1}$, to avoid breaks during the discontinuity following task. The inhibition levels $I_{(v,k)}$ for each cell v are defined in Eq. (10), considering $\alpha = 1.01$ and $\beta = 9$ (corresponding plot presented in Fig. 8 a)). Parameter d is given by $d = d_k/d_{max}$, where d_k expresses the Euclidean distance between o_k and $\hat{o}_{k-1}$, and d_{max} is a constant representing the maximum possible distance between o_k and $\hat{o}_{k-1}$ for the workspace dimensions. Θ is a normalisation constant. The values of $I_{(v,k)}(d)$ range from 0 to 1, with $I_{(v,k)} = 0$ indicating that the inhibition-of-return mechanism applies no inhibition to cell v, and $I_{(v,k)} = 1$ signalling full inhibition of cell v.

The selection of the region O_k of the workspace is also dependent on mechanisms that prevent returning to regions already explored and perceived with low uncertainty. In a nutshell, these mechanisms are formulated to promote the "curiosity", and are represented by the continuous random variable $U_{(v,k)}$ ="Uncertainty level for cell v", described as

$$U_{(v,k)} = \frac{\mathscr{H}(M_{(v,k)})}{max(\mathscr{H}(M_{(v,k)}))}, \quad U_{(v,k)} \in [0,1], \qquad (11)$$

in which the operator $\mathscr{H}$ determines the information entropy [30] of the discrete random variable $M_{(v,k)}$.

Another factor conditioning the determination of O_k is the saliency of the haptic stimulus for region v as comparing to its surroundings. Besides depending on the perceived haptic stimulus $M_{(v,k)}$ map, the formulation of the saliency of haptic stimuli is also modulated by the current objectives of the exploration task. The objectives of the task being executed by the robotic platform are represented by the discrete random variable T ="Task objective.", given that $T \in \{T_1, \ldots, T_\Phi\}$. During an experimental run the value of $T = t$ is considered constant throughout. Φ expresses the total number of different tasks that can be executed by the robotic platform.

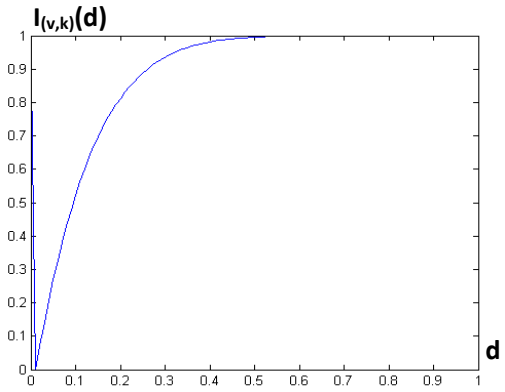

(a)

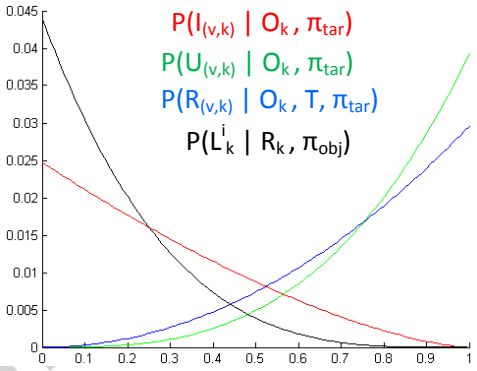

(b)

Figure 8: Graphical representation of: a) $I_{(v,k)}$. b) $P(I_{(v,k)}|O_k, \pi_{tar})$, $P(U_{(v,k)}|O_k, \pi_{tar})$, $P(S_{(v,k)}|O_k, T, \pi_{tar})$, $P(l^i_k|R_k, \pi_{obj})$.

Based on these considerations, the saliency of the haptic stimulus at v is denoted by continuous random variable $S_{(v,k)}$, and is dependent on the class of tasks T="*Search and follow of discontinuities between regions of surfaces with Material$_a$ and Material$_b$.*". $S_{(v,k)}$ is related by a soft evidence relation with the perceived haptic stimulus $M_{(v,k)}$ characterisation of the workspace (detailed description in [3]) given by

$$S_{(v,k)} = \frac{\max(|s_x|, |s_y|, |s_z|)}{s_{norm}}, \quad S_{(v,k)} \in [0,1] \qquad (12)$$

The parameters $s_x = \mathscr{G}_{sobel_x}(\mathbf{d})$, $s_y = \mathscr{G}_{sobel_y}(\mathbf{d})$ and $s_z = \mathscr{G}_{sobel_z}(\mathbf{d})$ are determined using a 3×3 edge detector $\mathbf{G}_{sobel}$ (3×3 kernel around v) following an approach described in [3] [31]. High values of $S_{(v,k)}$ correspond to regions around v expressing a haptic discontinuity between $Material_a$ and $Material_b$.

5.2. Inference of the next exploration target

Based on the conditional independence relations between random variables O_k, $I_{(v,k)}$, $U_{(v,k)}$, R_k $S_{(v,k)}$, T, presented in Fig. 7 a), the joint probability distribution function $P(O_k, T, S_{(v,k)}, U_{(v,k)}, I_{(v,k)}, R_k|\pi_{tar})$ for this model π_{tar}, is decomposed as summarised in Fig. 7 b), including parametric forms corresponding to each factor. The final estimate for the next exploration target $\hat{o}_k$ is given using a *Maximum a Posteriori* (MAP) decision rule, given a specific task $T = t$, as follows

$$\hat{o}_k = \arg\max_{o_k} P(O_k|t, s_{(v,k)}, i_{(v,k)}, u_{(v,k)}, R_k, \pi_{tar}) \Leftrightarrow$$

$$\hat{o}_k = \arg\max_{o_k} \sum_{R_k} \begin{pmatrix} P(t|\pi_{tar}).P(i_{(v,k)}|O_k, \pi_{tar}).P(O_k|\pi_{tar}). \\ P(s_{(v,k)}|O_k, t, \pi_{tar}).P(u_{(v,k)}|O_k, \pi_{tar}). \\ P(R_k|O_k, \pi_{tar}) \end{pmatrix} \quad (13)$$

The determination of the probability distribution functions $P(S_{(v,k)}|O_k, T, \pi_{tar})$, $P(I_{(v,k)}|O_k, \pi_{tar})$, $P(U_{(v,k)}|O_k, \pi_{tar})$, $P(R_k|O_k, \pi_{tar})$ involved in equation (13) is described in detail next.

5.3. Determination of $P(S_{(v,k)}|O_k, T, \pi_{tar})$, $P(I_{(v,k)}|O_k, \pi_{tar})$, $P(U_{(v,k)}|O_k, \pi_{tar})$, $P(R_k|O_k, \pi_{tar})$

As presented in Fig. 7 b), $P(I_{(v,k)}|O_k, \pi_{tar})$ is described by a beta probability distribution function $\mathscr{B}_I$ characterized by the constants $\alpha_I = 1$ and $\beta_I = 2.5$. The profile of the probability distribution function $P(I_{(v,k)}|O_k, \pi_{tar})$ is represented in Fig. 8 b). The selected profile for $P(I_{(v,k)}|O_k, \pi_{tar})$ attributes higher probabilities to lower levels of $I_{(v,k)}$ and lower probabilities to higher values of $I_{(v,k)}$ in order to promote the selection of regions of the workspace with low values of inhibition level.

Following an analogous approach, $P(U_{(v,k)}|O_k, \pi_{tar})$ is described by a beta probability distribution function $\mathscr{B}_U$ (Fig. 8 b)) with the constant parameters $\alpha_U = 4$ and $\beta_U = 1$. $P(U_{(v,k)}|O_k, \pi_{tar})$ attributes higher probability values to regions of the workspace perceived with higher uncertainty $U_{(v,k)}$, promoting the curiosity of the system.

$P(S_{(v,k)}|O_k, T, \pi_{tar})$ is described by a beta probability distribution function $\mathscr{B}_R$ defined by $\alpha_R = 3$ and $\beta_R = 1$ (Fig. 8 b)), assigning higher probability values to workspace regions v with higher values of saliency $S_{(v,k)}$, promoting the exploration of regions of the workspace with relevant haptic stimulus for the task under execution.

The probability distribution function $P(R_k|O_k, \pi_{tar})$ is defined as a Gaussian Mixture Model (GMM), as follows

$$P(R_k = "Object_j"|O_k, \pi_{tar}) = \sum_{i \in template'_j} w_i.g_i(O_k|\mu_i, \Sigma) \quad (14)$$

The Gaussians g_i of the GMM are centred at the locations μ_i of the workspace, with a covariance matrix Σ. Assuming a 2-D structure of the workspace, each Gaussian function g_i is defined as follows:

$$g_i(O_k|\mu_i, \Sigma) = \frac{1}{2\pi^{(3/2)} \mid \Sigma \mid} \exp^{-\frac{1}{2}(O_k - \mu_i)\Sigma^{-1}(O_k - \mu_i)}. \quad (15)$$

The centers μ_i of the Gaussians correspond to the points belonging to the set $Template'_j$, which are determined as presented in detail in section 4.

6. Experimental results

6.1. Computational simulation

The path planning method proposed by this work, supporting the global haptic exploration strategy, was simulated computationally using *MATLAB*. The simulation scenario consists on a planar 2D probabilistic grid representing the workspace placed in front of a hypothetical robotic platform, as represented in figure 9. Three different materials were used: wood ($Material_{10}$, brown cells), silicone ($Material_8$, blue cells) and flush ($Material_7$, green cells). The spatial distribution of the three materials intends to simulate an hypothetical real world scenario shown in figure 9. The workspace grid has the following lower and upper dimensions respectively $X_l^W = 0m$, $X_u^W = 0.30m$, $Y_l^W = 0m$, $Y_u^W = 0.60m$. Each cell (square) has a side dimension of $\varepsilon = 0.01m$. This work considers that all the regions of the workspace are reachable by a robotic exploratory element.

As detailed previously in section 1.2, this work does not address the low-level (motor and sensing) control loop involved in physical interaction between robotic fingers and surface. In the computational simulation, the sensory features modelling the haptic properties, texture ($E_{(v,k)}$) and compliance ($C_{(v,k)}$), of materials $Material_7$, $Material_8$, $Material_{10}$, were extracted from a previous work [10], as detailed in section 3.

6.2. Autonomous exploration of the workspace

This work assumes that at each time iteration step k of the system illustrated in figure 3, an exploratory element of a robotic hand probes a workspace region v. The sensory samples modelling texture $e_{(v,k)}$ and compliance $c_{(v,k)}$ are artificially synthesised from the respective probability distribution functions $P(E_{(v,k)}|m_{(v,k)}, \pi_{per})$ and $P(C_{(v,k)}|m_{(v,k)}, \pi_{per})$, given the known ground truth material $m_{(v,k)}$ for that region of the workspace, as defined in figure 9. Following the architecture of the sensory processing pipeline represented in figure 3, the sensory features samples $e_{(v,k)}$, $c_{(v,k)}$ are integrated by the Bayesian models to infer the next region (via point) of the workspace that should be probed by a robotic system.

In this scenario, the exploratory element of the robotic system initialized ($k = 0$) at random locations of the bi-dimensional grid representing the workspace region. The full-list of initialization locations for the 100 runs, is available online at `http://www.rmartins.net/j2016a`. Unlike in previous work [3], these cells of the grid are not only located on a haptic discontinuity between the different materials of the scenario; they

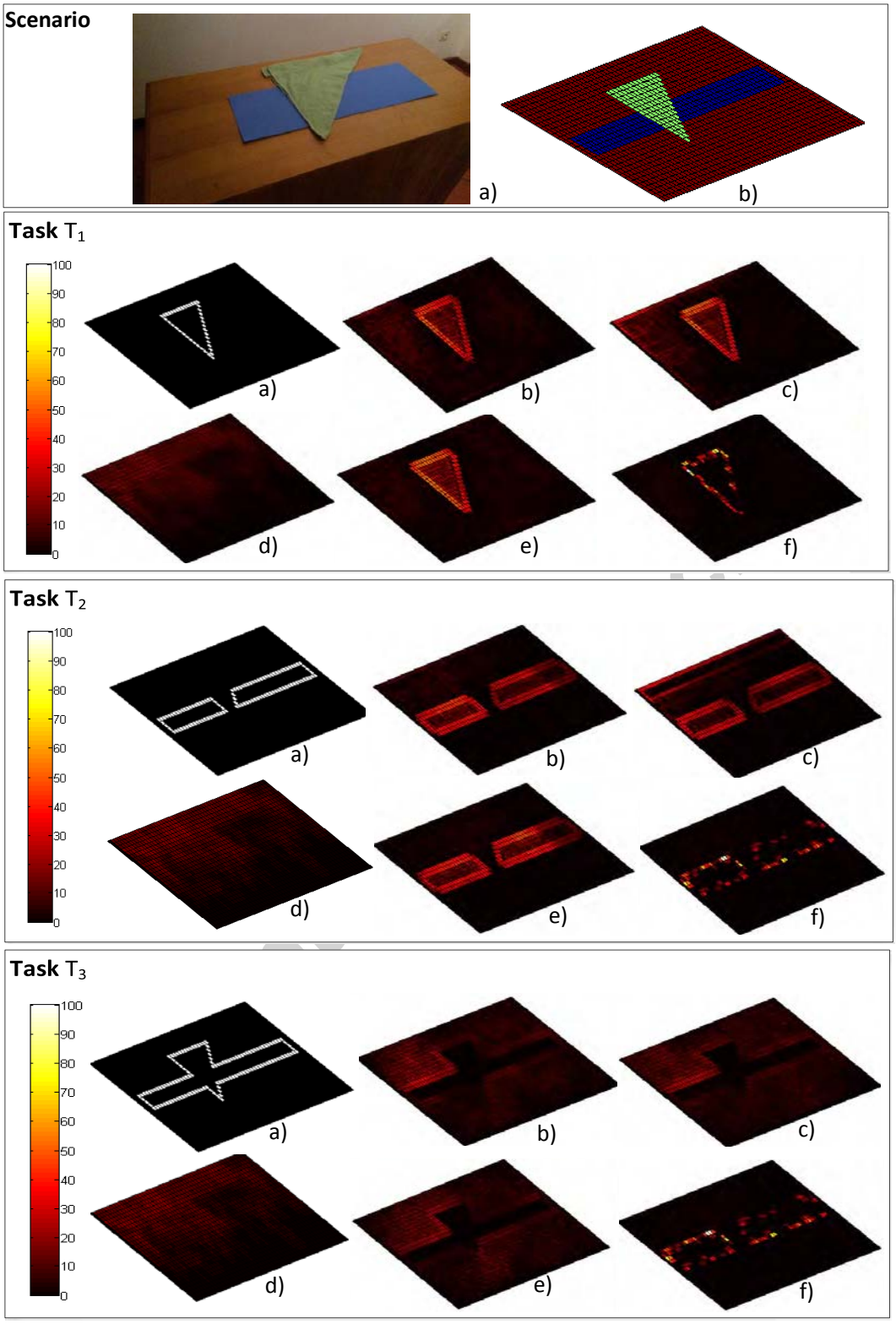

Figure 9: Scenario: a) Real world representation of the scenario. b) Schematic representation of configuration of the haptic stimulus placed in the workspace. The materials wood ($Material_{10}$), silicone ($Material_8$) and flush ($Material_7$) are represented in brown, blue, green respectively. c) Representation of the workspace in the virtual environment. Tasks: a) Ground truth exploration path for the respective task. b)-f) Heat map of the exploration paths after 100 exploration runs with a duration of 100 time iterations each. Different exploration behaviours by integrating different configurations of the Bayesian model π_{tar}: b) full-model c) removing shape cues R_k d) removing haptic saliency $S_{(v,k)}$ e) removing inhibition-of-return mechanisms $I_{(v,k)}$ f) removing uncertainty cues $U_{(v,k)}$.

can be located on homogeneous regions. This provides a completely blind and unbiased initialization of the exploration task for each exploration run.

During each exploration task, the workspace presented in the Fig. 9 was explored during 100 runs (100 different initial locations of the exploratory element). For each run, the exploration procedures lasts 100 iterations (emulating time steps in realistic conditions) $k = 0 \ldots 99$.

6.2.1. Exploration tasks

To evaluate the specificity and robustness of the Bayesian models implementing the touch attention mechanisms proposed in this work, the autonomous exploration of the workspace was performed using three different tasks (T_1, T_2,T_3). The objectives are the following T_1="search and follow of discontinuities between $Material_7$ and remaining materials"; T_2="search and follow of discontinuities between $Material_8$ and remaining materials"; T_3="search and follow of discontinuities between $Material_{10}$ and remaining materials";

6.2.2. Performance metric

Although the internal structure and configuration of the haptic stimulus disposed in the workspace is unknown *a-priori* to the robotic system, the ground truth describing the target locations (grid cells) of the workspace that should be probed by the robotic platform during task execution can be defined by a human operator for benchmarking purposes, and is denoted as $\mathscr{B} = \{\mathbf{b}_1, \mathbf{b}_2, \mathbf{b}_3, \ldots, \mathbf{b}_l\}$, $\mathbf{b}_i = (x, y) \in \mathbb{R}^2$. The set of workspace regions actually probed by the robotic platform during task execution, on the other hand, is denoted as $\mathscr{V} = \{\mathbf{v}_1, \mathbf{v}_2, \mathbf{v}_3, \ldots, \mathbf{v}_k\}$, $\mathbf{v}_i = (x, y) \in \mathbb{R}^2$.

The performance of the autonomous execution of the task by the robotic platform during an experimental run can be evaluated by the following error metric:

$$\Gamma = \sum_{i=1}^{l} \|\mathbf{b}_i - \mathbf{v}_{nearest}\|, \quad \text{given that}$$
$$\forall_{\mathbf{v}_i \in \mathscr{V}} \quad \exists_{\mathbf{v}_{nearest}} : \|\mathbf{b}_i - \mathbf{v}_{nearest}\| \leq \|\mathbf{b}_i - \mathbf{v}_i\|, \qquad (16)$$

where $\| \ldots \|$ represents the Euclidean distance operator. This metric determines the total Euclidean distance between each ground truth point and the nearest point belonging the exploration path executed by the robotic platform. According to this approach, better autonomous exploration strategies provide lower values of Γ.

6.3. Discussion of the experimental results

The impact of the different components (discontinuity shape cues, uncertainty, haptic saliency, inhibition-of-return) of the Bayesian models implementing the touch attention mechanisms was evaluated by comparing the exploration performance after discarding specific components of the Bayesian model π_{tar}: shape cues R_k, haptic saliency $S_{(v,k)}$, inhibition-of-return mechanisms $I_{(v,k)}$, uncertainty cues $U_{(v,k)}$. The influence of those

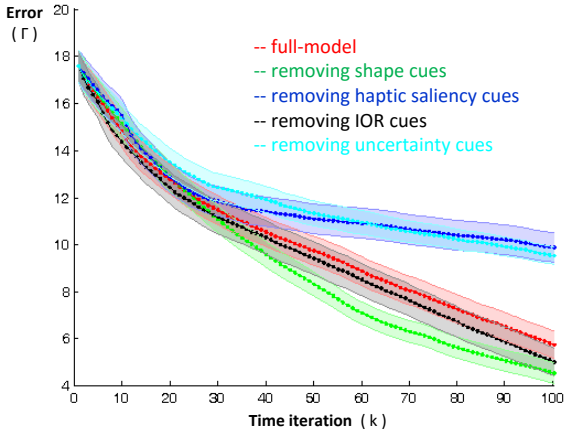

(a)

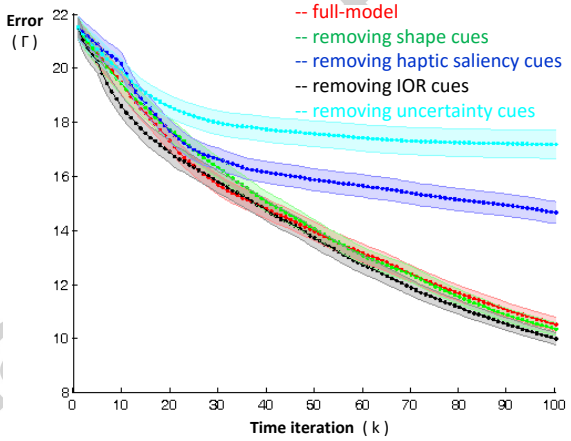

(b)

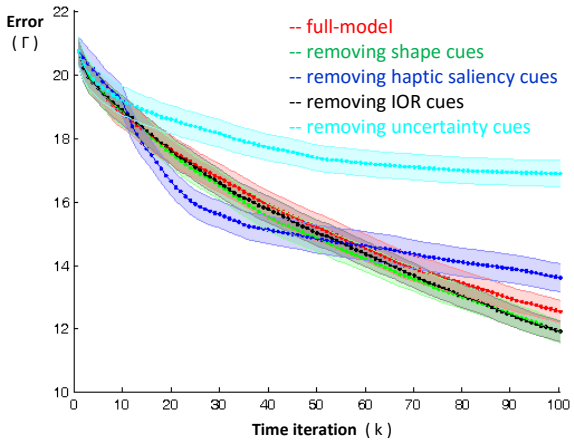

(c)

Figure 10: Temporal evolution (from $k = 0$ to $k = 100$) of mean value (average for the 100 runs; shaded colors represent SEM: standard error of mean) of performance metric Γ by integrating different configurations of Bayesian model π_{tar}: full-model, removing shape cues R_k, removing haptic saliency $S_{(v,k)}$, removing inhibition-of-return mechanisms $I_{(v,k)}$, removing uncertainty cues $U_{(v,k)}$. a) Task T_1. b) Task T_2. c) Task T_3.

components was discarded by assuming that each of those random variables is described by a uniform probability distribution throughout the respective experimental runs.

Animated representations (time lapse) of the probability distribution functions during 100 time iterations involved in the progressive inference by the Bayesian model π_{tar} of the workspace region that should be explored next, are available online at `http://www.rmartins.net/j2016a`, and an example is illustrated in Fig. 11.

The ground truth exploration paths for the objectives of the exploration tasks T_1, T_2 and T_3 are illustrated in Fig. 9 representing the borders of the $Material_7$, $Material_8$ and $Material_{10}$ with the remaining materials in the workspace, respectively.

By performing a qualitative comparison between the ground truth exploration paths and the heat maps resulting from the exploration behaviour inferred by the full Bayesian model π_{tar} in the Fig. 9, one finds that there is a high correspondence between the spatial structure of the most explored regions and the spatial structure of the ground truth exploration paths. The performance metric presented in Fig. 10 also shows that the full model always provides a good result. The touch attention mechanisms implemented by the Bayesian model π_{tar} have promoted the exploration of regions corresponding to the discontinuities described in the objectives of the tasks T_1, T_2, T_3, ignoring other types of haptic discontinuities.

The structural correspondence is higher for T_1 and T_2. This better performance is justified by the better perceptual discrimination capability of this system concerning $Material_7$ and $Material_8$ relatively to $Material_{10}$ (extensive study in [3]).

The analysis of the results of discarding the influence of specific components of the Bayesian model π_{tar} (Fig. 9), shows that the degradation of performance of the exploration behaviour is significant (Fig. 10) when the effect of the haptic saliency $S_{(v,k)}$ is not considered. This causes the system to explore randomly the workspace, not taking into consideration any information about task relevance concerning the sensed haptic stimulus.

By neutralising the integration of the information about the uncertainty of the perceptual representation of the workspace (Fig. 9), the robotic system fails to have an exploration strategy that produces results similar to the ground truth. Although the Bayesian model π_{tar} implements inhibition-of-return mechanisms, their effect is transient, and therefore, after some time elapses, the system tends to return to the same regions of the workspace that have been explored previously and were perceived with low uncertainty, thus providing a high saliency score for the task being executed. The plot of the performance metric Γ for those conditions, shows that the degradation of performance of the exploration behaviour is considerable (Fig. 10).

By disabling the integration of the effects of the inhibition-of-return mechanisms, exploration task execution performance is less degraded. The plots of the Γ metric, presented in Fig. 10, support this evidence by showing a performance of the system at the same level as the full-model condition. The removal of the transient effect of the inhibition-of-return mechanisms is compensated by the integration of information of mechanisms related with the uncertainty of the perceptual representation of the workspace, which naturally correspond to less explored regions, if all surfaces in the workspace remain static/rigid. These regions tend to be avoided by the system, even without the influence of the inhibition-of-return mechanisms. The inhibition-of-return mechanisms may play a more relevant role in more ambiguous scenarios made of materials that the system can only perceive with high uncertainty, even after considerable exploration.

Discarding the effects provided by the integration of shape cues (Fig. 9), does not have a strong influence in the performance of the exploration behaviour of the system (Fig. 10). The weak contribution of the shape cues of the discontinuity to the improvement of the performance of the robotic system was caused by the low number of shape primitives recognized in this work (only two: rectangle and triangle) and by the high number of points that were used to describe each of the templates (around 50 points).

7. Conclusions and future work

The integration of touch attention mechanisms in the exploration of surfaces by robotic hands proved to be effective to search and follow haptic discontinuities based on noisy sensory data describing unknown scenes. The updated perceptual representation of the workspace, provided by the Bayesian model π_{per}, together with shape cues about the structure of the discontinuity being followed provided by the Bayesian model π_{obj} (extension of previous work [3]), are integrated by the Bayesian model π_{tar} to perform perceptual inference and drive the decision process to determine the region that should be explored in the subsequent time step.

The Bayesian models were tested in a simulated scenario including three different materials during three different haptic exploration tasks. The results presented in section 6.2, have demonstrated that the proposed approach provides the robotic system with a useful framework to define and generalise exploration behaviours. As in [22], the system was able to deal with severe changes in the slope of the discontinuities. In all the tasks, the robotic system was able to follow haptic discontinuities with progressive inversions in the slope of the discontinuity, what clearly demonstrates the generalization capability of the proposed approach. The emergent behaviour displayed by the system offers an improvement on the results presented in [22]. Testing the system with slope variations in discontinuities other than right angles (90 degrees) was suggested by [22] as a relevant future course of work.

The touch attention mechanisms proposed in this work also showed high specificity. The robotic system followed the haptic discontinuities between the materials of interest for each task, ignoring other haptic discontinuities.

According with the results presented in section 6.2, the performance of the robotic system during the haptic exploration tasks is heavily dependent on the integration by the Bayesian model π_{tar} of information about the haptic saliency $S_{(v,k)}$ and uncertainty $U_{(v,k)}$ of the perceptual representation of the workspace. The formulation of the contributions of the inhibition-of-return mechanisms $I_{(v,k)}$ and shape cues of the haptic discon-

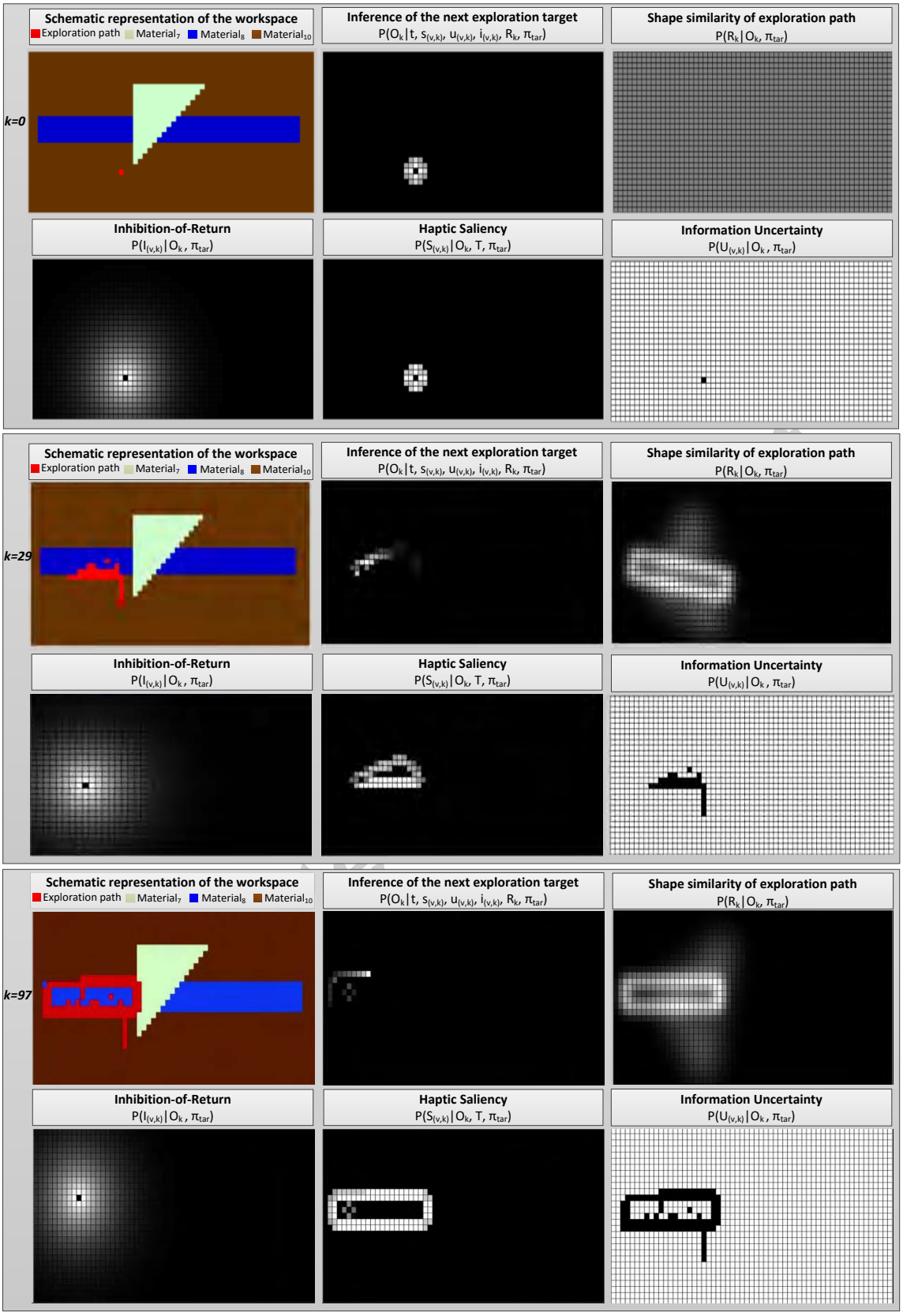

Figure 11: Representation of the $P(I_{(v,k)}|O_k,\pi_{tar})$, $P(S_{(v,k)}|O_k,T,\pi_{tar})$, $P(U_{(v,k)}|O_k,\pi_{tar})$, $P(R_k|O_k,\pi_{tar})$, $P(O_k|t,r_{(v,k)},i_{(v,k)},u_{(v,k)},r_k,\pi_{tar})$ probability distribution functions and the exploration behaviour during the execution of the task T_2 *search and follow of discontinuities between* $Material_8$ *and remaining materials*, run 18. Dark colors represent lower values. Light colors represent higher values. Animated versions of this type of representations for autonomous exploration tasks T_1,T_2 and T_3, are available on-line *www.rmartins.net/j2016a*.

tinuities R_k is going to be studied extensively in future work, in order to improve and optimize the contributions of these components of the Bayesian model to the performance of the robotic system. In future developments of this work, elementary shape primitives should be recognized by the system and alternatives methods to ICP should be tested. This will allow the system to recognize earlier the tendencies in the shape of the discontinuity, matching the current exploration path with the shape templates more robustly (noise, scale, orientation). The future developments of this work will also investigate the implementation of the automatic computational optimization of the parameters defining the profile of Beta distribution functions. Currently, the selection of parameters is made empirically, testing different sets of values and analysing the behaviour of the system.

In this work, the space used to formulate the solution of the global haptic exploration path planning consists in a 2D grid. The next developments of the proposed approach will study the extension of this space to a 3D grid. The operators and functions defined in 2D space during the formulation of the Bayesian models can be easily adjusted to 3D spaces (eg: exploration path matching with shape temples; Sobel operators involved in the formulation of haptic saliency; assignment of inhibition levels).

Acknowledgements

This research work was financially supported by an individual Ph.D. scholarship (SFRH/BD/65990/2009) funded by the Portuguese science agency FCT - Fundação para a Ciência e a Tecnologia (Foundation for Science and Technology).

References

[1] R. S. Johansson, J. R. Flanagan, Coding and use of tactile signals from the fingertips in object manipulation tasks, Nat Rev Neurosci 10 (2009) 345–359.

[2] S. J. Lederman, The intelligent hand: An experimental approach to human object recognition and implications for robotics and ai, AI Magazine 15 (1994) 774–785.

[3] R. Martins, J. F. Ferreira, J. Dias, Touch attention bayesian models for robotic active haptic exploration of heterogeneous surfaces, in: Proceedings of 2014 IEEE/RSJ International Conference on Intelligent Robots and Systems (IROS 2014), IEEE, Chicago, USA, 2014, pp. 1208–1215. doi:10.1109/IROS.2014.6942711.
URL http://rmartins.net/iros2014a

[4] F. Meng, B. Guo, M. Song, X. Zhang, Image fusion with saliency map and interest points, Neurocomputing 177 (2016) 1 – 8.

[5] S.-W. Ban, M. Lee, Selective attention-based novelty scene detection in dynamic environments, Neurocomputing 69 (1315) (2006) 1723 – 1727, blind Source Separation and Independent Component AnalysisSelected papers from the {ICA} 2004 meeting, Granada, SpainBlind Source Separation and Independent Component Analysis.

[6] R. B. Gomes, B. M. de Carvalho, L. M. G. Gonalves, Visual attention guided features selection with foveated images, Neurocomputing 120 (2013) 34 – 44, image Feature Detection and Description.

[7] M. O. Ernst, H. H. Bulthoff, Merging the senses into a robust percept, Trends in cognitive sciences 8 (2004) 162–169.

[8] E. Wacker, Tactile feature processing and attentional modulation in the human somatosensory system, PhD thesis TU Berlin.

[9] J. F. Ferreira, J. Dias, Probabilistic Approaches to Robotic Perception, Vol. 91 of Springer Tracts in Advanced Robotics, Springer, 2014.

[10] D. Xu, G. E. Loeb, J. A. Fishel, Tactile identification of objects using bayesian exploration, in: ICRA 2013, 2013.

[11] A. M. Okamura, M. R. Cutkosky, Feature detection for haptic exploration with robotic fingers, The International Journal of Robotics Research 20 (12) (2001) 925–938.

[12] C. M. Oddo, M. Controzzi, L. Beccai, C. Cipriani, M. C. Carrozza, Roughness encoding for discrimination of surfaces in artificial active-touch, IEEE Trans. Robotics 27 (3) (2011) 522–533.

[13] J. A. Fishel, G. E. Loeb, Bayesian exploration for intelligent identification of textures, Frontiers Neurorobotics 6.

[14] D. Chathuranga, V. Ho, S. Hirai, Investigation of a biomimetic fingertip's ability to discriminate fabrics based on surface textures, in: Int. Conf. Advanced Intelligent Mechatronics, 2013, pp. 1667–1674. doi:10.1109/AIM.2013.6584336.

[15] R. Martins, D. Faria, J. Dias, Representation framework of perceived object softness characteristics for active robotic hand exploration, in: HRI2012, USA, 2012.

[16] H. Liu, X. Song, J. Bimbo, L. Seneviratne, K. Althoefer, Surface material recognition through haptic exploration using an intelligent contact sensing finger, in: IROS 2012, IEEE, 2012, pp. 52–57.

[17] F. Castelli, An integrated tactile-thermal robot sensor with capacitive tactile array, IEEE T. Industry App. 38 (1) (2002) 85–90. doi:10.1109/28.980361.

[18] H. Liu, D. P. Noonan, B. J. Challacombe, P. Dasgupta, L. D. Seneviratne, K. Althoefer, Rolling mechanical imaging for tissue abnormality localization during minimally invasive surgery, Biomedical Engineering, IEEE Transactions on 57 (2) (2010) 404–414.

[19] L. L. Bologna, J. Pinoteau, J.-B. Passot, J. A. Garrido, J. Vogel, E. R. Vidal, A. Arleo, A closed-loop neurobotic system for fine touch sensing, Journal of Neural Engineering 10 (4).

[20] Q. Li, C. Schrmann, R. Haschke, H. Ritter, A control framework for tactile servoing, in: Proceedings of RSS, 2013.

[21] J. Bohg, M. Johnson-Roberson, M. Bjoandrkman, D. Kragic, Strategies for multi-modal scene exploration, in: Intelligent Robots and Systems (IROS), 2010 IEEE/RSJ International Conference on, 2010, pp. 4509 – 4515.

[22] U. Martinez-Hernandez, T. Dodd, L. Natale, G. Metta, T. Prescott, N. Lepora, Active contour following to explore object shape with robot touch, in: World Haptics 2013, 2013, pp. 341–346.

[23] L. D. Harmon, Automated tactile sensing, The International Journal of Robotics Research 1 (2) (1982) 3–32.

[24] R. L. Klatzky, S. J. Lederman, V. A. Metzger, Identifying objects by touch: An expert system, Perception & Psychophysics 37 (4) (1985) 299–302.

[25] P. Dario, D. De Rossi, Tactile sensors and the gripping challenge: Increasing the performance of sensors over a wide range of force is a first step toward robotry that can hold and manipulate objects as humans do, Spectrum, IEEE 22 (8) (1985) 46–53. doi:10.1109/MSPEC.1985.6370785.

[26] H. R. Nicholls, M. H. Lee, A survey of robot tactile sensing technology, The International Journal of Robotics Research 8 (3) (1989) 3–30.

[27] R. S. Dahiya, G. Metta, M. Valle, G. Sandini, Tactile sensing - from humans to humanoids, Robotics, IEEE Transactions on 26 (1) (2010) 1–20.

[28] Z. Zhang, Iterative point matching for registration of free-form curves and surfaces, International journal of computer vision.

[29] J. F. Ferreira, J. Dias, Attentional mechanisms for socially interactive robots - a survey, IEEE Transactions on Autonomous Mental Development, Special Issue on Behavior Understanding and Developmental Robotics (in press) (2014) 1–18.

[30] C. E. Shannon, A mathematical theory of communication, SIGMOBILE Mob. Comput. Commun. Rev. 5 (1) (2001) 3–55.

[31] P. Bhattacharya, D. Wild, A new edge detector for gray volumetric data, Computers in Biology and Medicine 26 (4).